*Advanced Materials Interfaces*

ADVANCED MATERIALS INTERFACES Open Access

www.advmatinterfaces.de

RESEARCH ARTICLE OPEN ACCESS

# Influence of the Substrate Temperature on the Growth Mechanism of Allylamine Plasma Polymer Films

Robin Dantinne[1] | Nathan Vinx[1] | Philippe Leclère[2] | Damien Cossement[3] | Claude Poleunis[4] | Arnaud Delcorte[4] | Damien Thiry[1]

[1]Chimie des Interactions Plasma-Surface (ChIPS), Research Institute for Materials Science and Engineering, University of Mons, Mons, Belgium | [2]Laboratory for Physics of Nanomaterials and Energy (LPNE), Research Institute for Materials Science and Engineering, CIRMAP, University of Mons, Mons, Belgium | [3]Materia Nova Research Center, Parc Initialis, Mons, Belgium | [4]Institute of Condensed Matter and Nanosciences (IMCN), Université Catholique De Louvain (UCL), Louvain-la-Neuve, Belgium

**Correspondence:** Robin Dantinne (robin.dantinne@umons.ac.be)

**Received:** 30 October 2025 | **Revised:** 14 February 2026 | **Accepted:** 22 March 2026

**Keywords:** allylamine | glass transition | growth mechanism | plasma polymer | substrate temperature

## ABSTRACT

This work aims to investigate the impact of the substrate temperature on the growth mechanism of allylamine-based plasma polymer films (PPF). A comprehensive study of the PPF physicochemical properties, including the mechanical properties, the glass transition temperature, the chemical composition, the cross-linking degree and the deposition kinetics, is performed and correlated to plasma chemistry. As the substrate temperature evolves from -10°C to 45°C, the glass transition temperature is observed to increase from 75°C to 230°C. This evolution is correlated to an increase in cross-linking degree, modulated by the energy density brought by ion bombardment during film growth. The energy density is, in turn, significantly influenced by the deposition kinetics which strongly depend on the thermal conditions of the substrate, as evidenced by the growth rate decrease from 5.4 to 1.6 nm/min with the substrate temperature. Similarities are observed with another allyl-based PPF family, suggesting a comparable growth mechanism but distinct film properties attributed to differences in growth rate. Overall, this study highlights the combined role of precursor chemistry and substrate temperature as key parameters for fine tuning of plasma polymer film properties.

## 1 | Introduction

Over the past four decades, plasma polymer films (PPFs) bearing reactive functional groups such as thiols (—SH) [1], amines ($—NH_2$) [2], hydroxyls (—OH) [3] or carboxyls (—COOH) [4] have attracted considerable attention for applications ranging from biosensor fabrication [5] and antibacterial coatings [6] to nanoparticle stabilization [7]. In plasma polymerization, an organic precursor is activated in a discharge, generating a variety of reactive species (ions and mainly radicals) that condense on exposed surfaces to form an organic thin film referred to as a plasma polymer. Their complex growth mechanism involving numerous surface and gas phase reactions is responsible for the unique structure of PPF distinguished by the absence of repeating monomeric units, as well as their outstanding properties including good thermal stability, insolubility in most solvents, and excellent adhesion properties on a large range of substrates. These properties as well as the industrial scalability of the process justify

**Abbreviations:** $NH_2$-$PPF_{X°C}$, PPF synthesized with allylamine at a substrate temperature "X" °C; PCA, Principal Component Analysis; PF-QNM, Peak-Force Quantitative Nanomechanical Mapping; PPF, Plasma Polymer Film; ToF-SIMS, Time-of-Flight Secondary Ions Mass Spectrometry; $T_S$, substrate temperature; $T_T$, surface transition temperature; XPS, X-ray Photoelectron Spectroscopy; $\chi$, cross-linking degree.

the increasing interest in the plasma polymerization technique [8–10].

The technique also offers an exceptional flexibility. Indeed, by a judicious selection of the process parameters, one can tailor the PPF physicochemical properties to meet specific application requirements. To date, research has primarily focused on the energy invested per particle in the plasma governing the precursor fragmentation [11–13]. These investigations show that lower energy conditions favor the preservation of precursor functionality and leads to lower cross-linking density.

First highlighted by Yasuda in the 1980s, the substrate temperature ($T_S$) which dictates the adsorption–desorption equilibrium at the growing film interface has been less explored [14, 15]. Although it could be expected that increasing $T_S$ would promote radical surface recombination, early studies on hydrocarbon and fluorocarbon-based PPFs demonstrated that higher $T_S$ results in a decrease in deposition kinetics by favoring the desorption of the film-forming species [15]. This behavior can be rationalized by comparing the energy barrier of the competing processes: since radical surface diffusion and subsequent recombination usually exhibit lower energy barriers than desorption, the latter will be more significantly influenced by $T_S$.

More recently, our group has conducted an extensive investigation regarding the substrate temperature influence on the chemical and mechanical properties of various plasma polymer families, including propanethiol, propylamine, allyl alcohol and propanol [16–18]. For some precursors such as allyl alcohol and propanethiol, the thermal condition of the substrate strongly influences the growth mechanism of the PPF. Notably, the adsorption-dependent growth rate impacts the density of energy delivered to the growing film, a key parameter to control the cross-linking degree of plasma polymers. The latter, in turn, has a pronounced impact on the PPF glass transition temperature governing their viscoelastic properties. These insights opened up new possibilities for the development of mechanically responsive films and related applications, including the exploitation of the spontaneous wrinkling phenomenon for the facile fabrication of PPF/metal nanostructured bilayers, which shows promising potential in flexible electronics [18–21]. In contrast, for other precursors like propanol and propylamine, the impact of the substrate temperature is considerably less pronounced.

In this context, the present work further extends our examination of the substrate temperature influence on the growth mechanism of PPF by investigating an additional nitrogen-based precursor, namely allylamine. This precursor has been extensively studied in the literature and the derived PPFs have found various attractive applications including enhanced cell proliferation and osteogenic differentiation. These biological properties are often attributed to the presence of charged amino groups at physiological pH-value or the influence of surface chemistry on key protein conformations [22, 23]. Beyond their applicative potential, studies of nitrogen-containing precursors have provided meaningful insights into the growth mechanism of plasma polymerization [17]. Structurally, nitrogen differs from other widely studied heteroelements, such as oxygen or sulfur, due to its higher valence (i.e. three for N, two for O and S) [24]. This can drastically affect both mechanical properties and the intrinsic cross-linking degree of the deposited PPF, thereby motivating a fundamental study of allylamine plasma polymerization and its comparison with allyl alcohol.

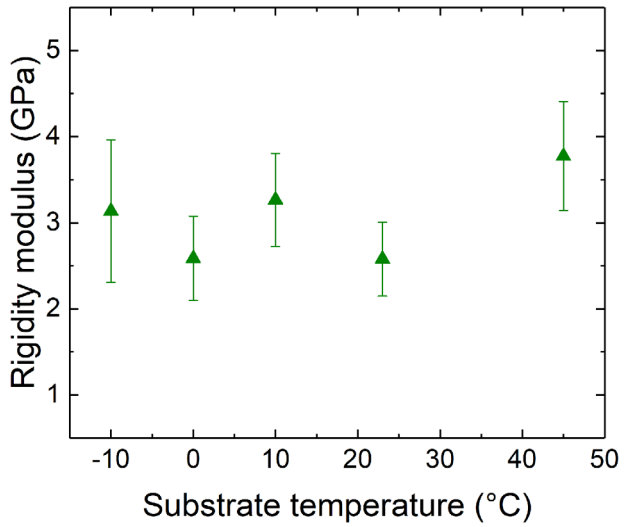


**FIGURE 1** | Evolution of the rigidity modulus for allylamine-based PPF as a function of the substrate temperature.

Nevertheless, to the best of our knowledge, the impact of $T_S$ on their growth mechanism and hence the physico-chemical properties of the coatings remain unknown.

Our research strategy consists of a thorough characterization of the physicochemical properties of the coatings, namely their mechanical properties (by using cutting-edge scanning probe microscopy and spectroscopy), glass transition temperature (Time-of-Flight Secondary Ions Mass Spectrometry [ToF-SIMS]), chemical composition (X-ray Photoelectron Spectroscopy [XPS]), cross-linking degree (ToF-SIMS) and deposition kinetics, as well as the chemistry of plasma (mass spectrometry).

## 2 | Results and Discussion

The mechanical properties of $NH_2$-PPF have been evaluated with the AFM Peak-Force Quantitative Nanomechanical Mapping (PF-QNM) method [25]. Typical force-distance curves of these samples are presented in Figure S1. The rigidity modulus ($E_M$) characterizing the elastic behavior of the probed material is extracted by fitting these curves with the JKR model, which is best suited for low-modulus materials (i.e. a few GPa) and has already been applied to other plasma polymer films families [16–18, 26]. It should be mentioned that viscoelastic contributions can be considered negligeable due to the high frequency of the PF-QNM analysis (i.e. 2 kHz), thereby validating the use of a purely elastic model for the rigidity modulus determination. This measurement is assumed to be independent of the PPF topography as the root-mean-square (RMS) roughness is below 0.7 nm for all PPF. Figure 1 shows the evolution of $E_M$ for $NH_2$-PPF as a function of $T_S$.

Considering subtle $T_S$-dependent variations within the confidence interval, the rigidity modulus remains stable around

3 GPa regardless of $T_S$ (i.e. from -10°C to 45°C). This $E_M$ value corresponds to the ones typically reported in the literature for different precursors [16–18, 27].

It should be mentioned that the mechanical behavior of $NH_2$-PPF samples is significantly different to that of allyl alcohol-based plasma polymer previously investigated considering the same synthesis conditions, despite both precursors presenting the same hydrocarbon backbone [16]. Indeed, for a $T_S$ evolving in the range of -10°C to 45°C, alcohol-based PPF behave like a liquid viscous film at low $T_S$ and a hard elastic film at high $T_S$ while $NH_2$-PPF exhibit solid behavior regardless of $T_S$.

Considering conventional polymerization, the viscoelastic properties of a polymeric material obtained from the same monomer can vary, from a viscous liquid to an elastic solid, as a function of their glass transition temperature ($T_g$) [28, 29]. Therefore, the evaluation of $T_g$ can provide meaningful insight on the evolution of the mechanical properties regarding the source molecule and the $T_S$.

On this basis, $NH_2$-PPF glass transition temperatures have been evaluated thanks to a ToF-SIMS-based method recently developed by Poleunis et al. [18, 30]. Briefly, the technique consists of measuring the rate of backscattered $Ar_n^+$ ions from $Ar_{3000}^+$ clusters during ToF-SIMS measurements of the sample surface performed at various analysis temperatures. It was demonstrated that the $Ar_2^+/(Ar_2^+ + Ar_3^+)$ ratio presents a sigmoidal evolution as a function of the analysis temperature. The resulting curve inflexion point, named surface transition temperature ($T_T$), is directly correlated to the glass transition temperature as evaluated by conventional differential scanning calorimetry [30]. This method has been successfully applied to probe the surface transition temperature of several PPF families [16, 17]. As ToF-SIMS measurements probe the extreme surface of the sample (i.e. typically 1 nm), $T_T$ values are systematically higher than the bulk $T_g$ of a given polymer, with reported differences ranging from 5°C to 26°C depending on the polymer. Thus, although the $T_g$ of PPF are not directly measured with this method, it can be reasonably expected that $T_T$ and $T_g$ values will follow the same trends. It should also be noted that the PF-QNM technique investigates the sample top surface, with an indentation depth of ∼ 1.5 nm in the present work. Consequently, surface ToF-SIMS analysis are ideal to further investigate the mechanical properties reported on Figure 1.

A typical recorded curve for $NH_2$-PPF is depicted in Figure 2a and presents a sigmoidal shape in agreement with the literature.[15] Whatever the substrate temperature, the $T_T$ of $NH_2$-PPF is systematically higher (i.e. from 75 ± 15 to 230°C ± 20°C) than the room temperature, meaning that the coatings' AFM analysis was performed at a temperature below their $T_T$. This explains the elastic solid behavior observed for the PF-QNM measurements of $NH_2$-PPF whatever $T_S$ (Figure 1).

Considering a conventional polymer, it is well established that the mechanical properties and the glass transition temperature of the material can be drastically affected by its cross-linking degree and chemical composition [28, 31]. Therefore, to better understand the observed trend of $T_T$, the cross-linking degree and chemical composition of $NH_2$-PPF at various $T_S$ have been evaluated by means of ToF-SIMS and XPS, respectively.

Figure S2a,b present typical XPS survey spectra, revealing the presence of carbon, nitrogen and oxygen in $NH_2$-PPF. The incorporation of oxygen in the allylamine-based coating despite its absence in the source molecule has already been reported in the literature and is ascribed to post-synthesis oxidation reactions involving dioxygen and water from ambient air and trapped radicals from the PPF coating [32–34].

As presented in Figure 3, a nitrogen to carbon ratio (i.e. N/C) of 0.39 is measured for $T_S$ = -10°C, before falling down to a plateau at around 0.28 for $0 < T_S < 45$°C.

These values are close to the N/C ratio of the precursor (i.e. 0.33), as already reported for allylamine-based PPF synthesized at low energetic conditions [34–36]. This high retention of the heteroelement for allylic precursors is sometimes explained by conventional polymerization of the source molecule by radical addition to the double bond [3, 36]. However, allylic monomers such as allylamine are prone to degradative chain transfer, i.e. the migration of a hydrogen in alpha position resulting in the formation of a resonance-stabilized radical [37]. The latter is unlikely to propagate the polymer chain and will eventually recombine with another radical, ending the polymerization process. An example of degradative chain transfer considering allylamine is illustrated in Figure S3.

To evaluate the nature of the chemical bonds involved in the PPF structure, the envelopes of the C1s and N1s peaks have been fitted.

For the C1s fitting, four components related to C—C/C—H at 285.0 eV, C—NR (R: H or C) and C═N (amine or imine functions) at 286.0 eV, C≡N/C—O—H/C—O—C (nitriles, alcohol or ether functions) at 286.9 eV and C═O (carbonyl or aldehyde functions) at 287.7 eV were used.

N1s peaks are fitted with three components, although their attribution is often uncertain as a result of the plethora of functions presenting similar energies: a first subpeak is attributed to R-$NH_2$/R-NH-R (primary or secondary amines) at 398.3 eV and a second subpeak associated to $R_3N$/CN/C═NH/CO—NH (tertiary amines, nitriles, imines and amides) at 399.4 eV. The third component at 400.6 eV is associated to diverse oxygen-containing structures such as (CO)N(CO)/($CO_2$)N/C═N—OH (imide, carbamate and hydroxylamine functions). It should be mentioned that characteristic subpeaks associated with functional groups containing N and O atoms such as imide, amide or carbamate are not observed in the C1s peak fitting. This can be explained by the higher concentration of carbon compared to nitrogen atoms and thus, a lower fraction of carbon atoms involved in these functional groups, resulting in a difficulty to observe them through C1s fitting.

The choice and labeling of these functions are based on reported detailed investigation of $NH_2$-based PPF [3, 17, 35, 38, 39]. As usually reported in the literature, new functionalities (i.e., imines, nitriles) that are absent from the precursor structure are created following the numerous recombination and rearrangements

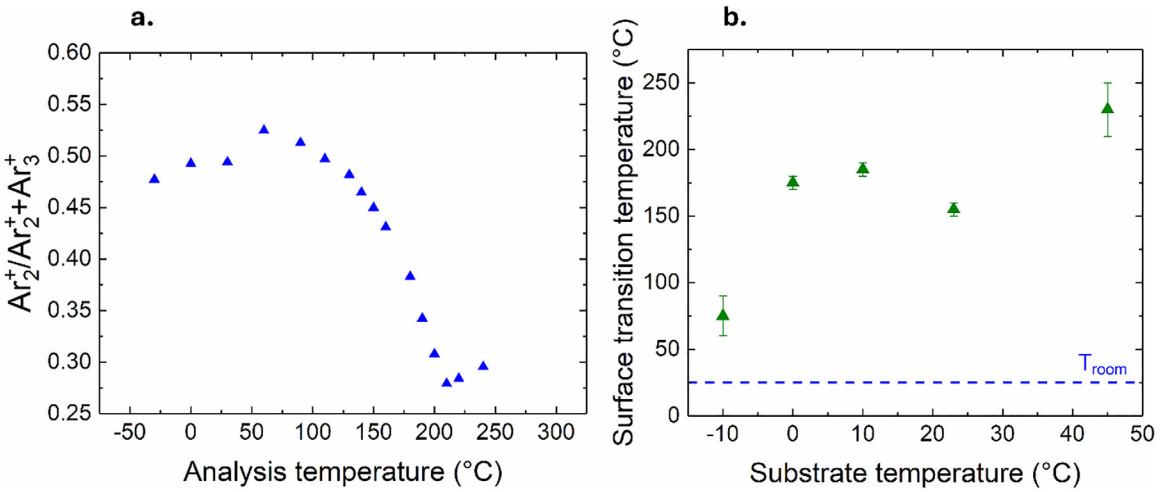


**FIGURE 2** | (a) $Ar_2^+/(Ar_2^+ + Ar_3^+)$ ratio of backscattered ions collected during the sputtering of $Ar_{3000}^+$ ions on the surface of $NH_2$-$PPF_{10°C}$. (b) The resulting curves are used to determine the surface transition temperature ($T_T$) of the coatings. The blue line shows the room temperature employed for analysis of mechanical properties.

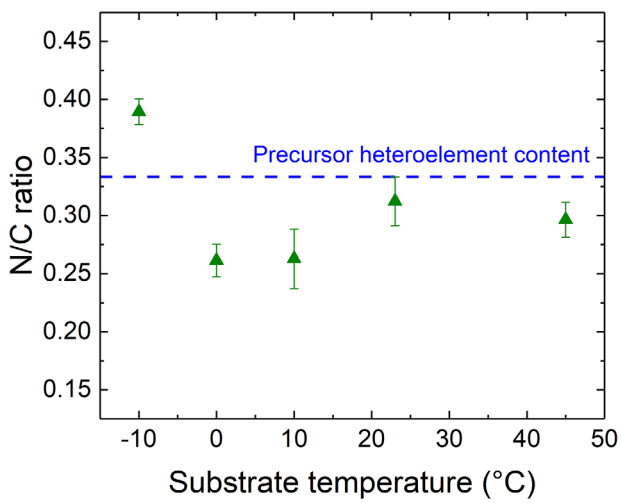


**FIGURE 3** | Evolution of the nitrogen to carbon ratio (N/C) of allylamine-based PPF with the substrate temperature.

reactions involved in the plasma polymerization process [3, 17, 38]. Components associated with C═O and other oxygen-containing functions clearly indicate the post-process oxidation of the PPF, as already highlighted in Figure S2.

A typical fitting procedure of the high-resolution C1s and N1s peaks for $NH_2$-PPF is presented in Figure 4a,b.

Figure 4c,d shows the evolution of the relative concentration of the different chemical groups with $T_S$. Considering the margin error, the relative concentration of each component remains rather stable with $T_S$ as already encountered for other plasma polymer families synthesized for similar experimental conditions [16, 17]. Consequently, the chemical composition of the PPF cannot explain the evolution of $T_T$ with $T_S$. In this context, the cross-linking degree of the PPF $\chi$, well-known to significantly influence the $T_g$ of conventional polymers, has been investigated by means of ToF-SIMS.

ToF-SIMS spectra of plasma polymer films usually present a plethora of peaks with various intensities, making extremely challenging the establishment of specific trends regarding the impact of $T_S$ on the PPF physicochemical properties. To overcome this problem, the PCA (Principal Component Analysis) has been used to extract the most important chemical and structural information of the ToF-SIMS spectra [40]. Previously, plasma polymerization studies have successfully evaluated the $\chi$ of various PPF using this method [27, 38, 41–43].

The "score" plot resulting from the PCA treatment of the $NH_2$-PPF ToF-SIMS data is presented in Figure 5. In this representation, every single point in the figure corresponds to a whole ToF-SIMS spectrum. The distance separating the points indicates variations between their corresponding spectra, revealing differences in the surface structure and/or chemistry. The ellipse drawn on the scores plot represents a 95% confidence interval. Considering our PCA analysis, it can be observed that most of the variance is represented by the *First Principal Component*, PC1 (i.e. 50.1%). Consequently, only PC1 is considered in the following discussion.

For each thermal condition, the spectra have formed small clusters according to $T_S$, although some clusters are more difficult to differentiate (e.g. $NH_2$-$PPF_{10°C}$ and $NH_2$-$PPF_{0°C}$). Therefore, the mean values of scores as a function of $T_S$ have been reported in Table 1 to rationalize their discrimination along PC1. Considering the confidence interval, it can be observed that the scores are well discriminated as a function of $T_S$ along the PC1, revealing a modification of $\chi$ and/or the chemical composition with $T_S$.

The most statistically important peaks called "loadings", i.e. peaks having a statistical weight > 90% in the PC1 model and responsible for the discrimination in the score plot, are reported in Table S1a,b. A positive or negative loading coefficient (corresponding to its statistical weight) is associated with each m/z signal. The absolute value of this loading coefficient is directly related to the relative intensity variation of the corresponding peak from one sample to another.

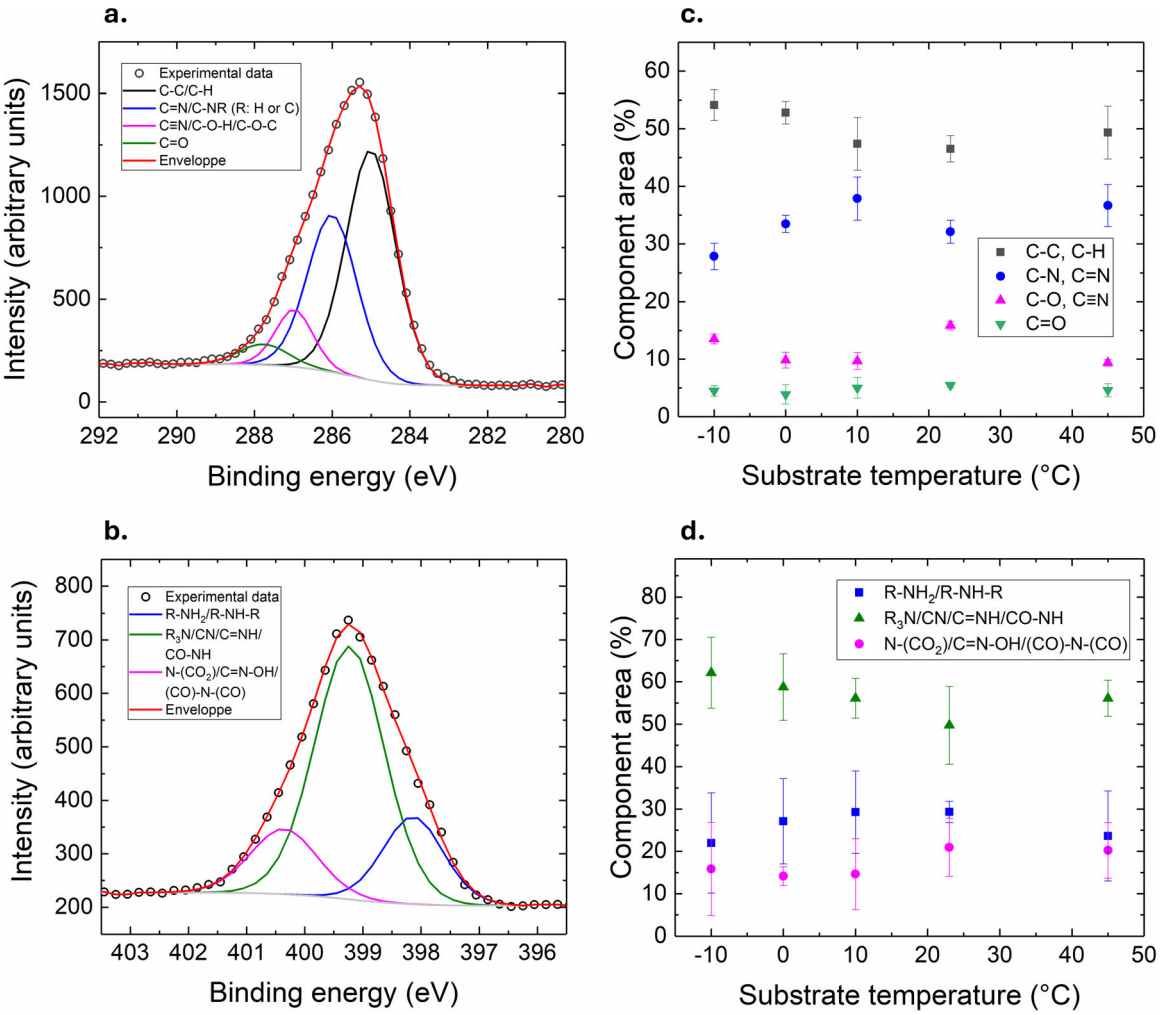


**FIGURE 4** | Typical fittings of high resolution C1s (a) and N1s (b) spectra for $NH_2$-$PPF_{0°C}$. Evolution of the component relative areas resulting from the fitting of the high-resolution C1s (c) and N1s (d) peaks of $NH_2$-PPF. For C1s fittings, four components are distinguished and associated with C—C/C—H (black), C—NR (R: H or C) and C═N (blue), C—O—H/C—O—C/C≡N (magenta) and C═O (green). Considering N1s peaks, three subpeaks are fitted and attributed to R-$NH_2$/R-NH-R (blue), $R_3N$/CN/C═NH/CO—NH (green) and N—($CO_2$)/C═N—OH/(CO)N(CO) (magenta).

To obtain information about $\chi$, the average chemical composition of the ionized fragments has been calculated for each loading category (negative and positive) [41]. In the first approach, each heteroelement present in these fragments has been replaced by an hydrocarbon group of identical valence state, i.e. CH and $CH_2$ groups for N and O atoms respectively. The corresponding data are presented in Table 2 for $NH_2$-PPF.

From the average fragment, particular attention is paid to the carbon to hydrogen ratio (C/H), strongly correlated with $\chi$ of the PPF [27]. It should be mentioned that the potential presence of unsaturation in the PPF (i.e. double/triple bonds or cycle) could also affect this ratio. However, FTIR analysis suggests a negligeable contribution of C═C bonds in the coating (Figure S4), as already demonstrated for several PPF families from (FT)IR analyses [44, 45]. Furthermore, XPS measurements clearly indicate that chemical functionalities of PPF are independent of the $T_S$, including unsaturated groups such as carbonyl or imine groups. Taking into account these considerations, it can be reasonably assumed that the influence of unsaturation over the C/H ratio is negligeable when varying $T_S$. Consequently, the C/H ratio is a reliable indicator of the PPF cross-linking degree. As observed from Table 2, the C/H ratio increases with $T_S$ (i.e., from 0.624 to 0.978), implying an increase in $\chi$ of the PPF with $T_S$. The latter correlates the evolution of $T_T$. Indeed, increasing $\chi$ effectively decreases the mobility of the molecular segments and thus increases $T_T$.

At this stage, it can be suggested that the increase of $\chi$ with $T_S$ mainly explains the evolution of $T_T$ as previously evidenced by ToF-SIMS measurements. However, the dependency of $\chi$ with $T_S$ remains unclear.

In order to further gather information about the growth mechanism of the PPF at a molecular level, mass spectrometry measurements in RGA mode were performed in order to identify the neutral species produced in the discharge. Indeed, it is accepted that the main species contributing to film growth are neutrals [46, 47]. The mass spectrum of allylamine plasma is depicted in Figure 6a.

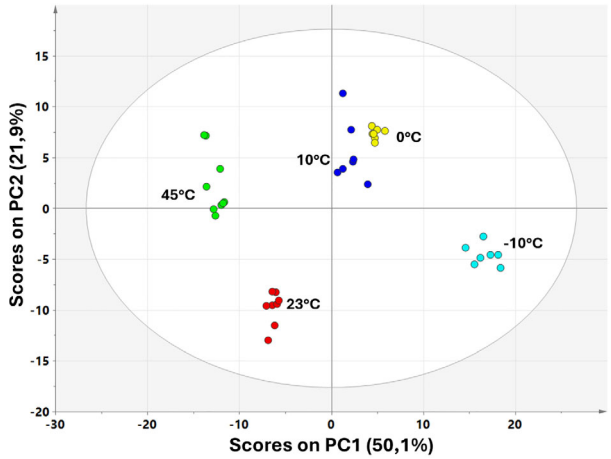


**FIGURE 5** | Score plot depicting sample discrimination based on the PCA processing of the positive ToF-SIMS data for $NH_2$-PPF.

Special attention is paid to the peak associated with the precursor (i.e. m/z = 57) as previous studies have established a correlation between the heteroelement concentration in the PPF and the concentration of non-fragmented monomer [2]. Therefore, the fragmentation degree of the allylamine precursor ($\alpha$) is calculated with the following equation:

$$\alpha = 1 - \frac{I_{prec.}\ (Plasma\ ON)}{I_{prec.}\ (Plasma\ OFF)} \quad (1)$$

where $I_{prec.}$ (Plasma ON) and $I_{prec.}$ (Plasma OFF) represents the experimental peak intensity for the precursor when the discharge is switched ON and OFF, respectively.

In our experimental conditions, a $\alpha$ value of 0.25 ± 0.05% is found correlating the high heteroelement content of $NH_2$-PPF as evaluated by XPS. Indeed, a lower fragmentation rate is usually associated to a higher functional group retention [2]. It should also be mentioned that the fragmentation rate influences the concentration of film-forming species in the plasma and thus likely impacts the growth kinetics, as it will be discussed later.

To achieve a deeper understanding of plasma chemistry, the mass spectra have been further analyzed. It should be emphasized that neutrals collected from plasma are ionized to enable their discrimination in the mass analyzer according to their m/z ratio. Newly formed ions can be produced in an excited state whose excess of energy can induce a fragmentation of the molecular ion, hence resulting in the appearance of additional peaks in the mass spectrum. This explains why a mass spectrum with several peaks is collected even when the plasma is not ignited as illustrated in Figure 6b. Therefore, except for the precursor, the presence of a given peak in the mass spectrum does not necessarily indicate that the corresponding specie is present in the plasma. On this basis, in order to take into account the fragmentation of the precursor in the mass spectrometer itself, signals recorded in the mass spectra of the plasma were corrected according to Equation 2 [48]:

$$I_c\ (m) = I_g\ (Plasma\ ON) - I_g\ (Plasma\ OFF).\frac{I_{prec.}\ (Plasma\ ON)}{I_{prec.}\ (Plasma\ OFF)} \quad (2)$$

where $I_c$ (m) is the corrected peak intensity for m/z = g, $I_g$ (Plasma ON) and $I_g$ (Plasma OFF) represent the experimental peak intensity for m/z = g when the plasma is switched ON and OFF, respectively. The corrected mass spectrum for allylamine plasma is presented in Figure 6c.

The main fragments identified in the mass spectra are summarized in Table 3. For clarity, ions corresponding to the precursor molecule missing one or more hydrogen atoms are denoted as $(M\text{-}xH)^+$, where x represents the number of hydrogen atoms removed from the source molecule. A plethora of signals are identified emphasizing the great diversity of species formed in the discharge (see Table 3 for the labeling). Carbon-based species—either containing nitrogen or not ($C_yH_xN_z$ and $C_yH_x$) and hydrogenated species associated with the heteroelement ($NH_x$) are observed. The presence of H and $H_2$ should also be mentioned as it could indicate surface recombination. It should be noted that discrimination between hydrocarbon and heteroelement-containing fragments is sometimes challenging given the isobaric interferences (e.g. m/z = 44 for $C_3H_8^+$ and $C_2H_6N^+$; m/z = 28 for $C_2H_4^+$ and $N_2^+$; m/z = 27 for $C_2H_3^+$ and $HCN^+$ or m/z = 16 for $CH_4^+$ and $NH_2^+$). Consequently, several peaks in the mass spectra can be attributed to multiple fragments, as one can see in Table 3.

Interestingly, a $(M\text{-}H)^+$ peak is clearly identified in the mass spectrum (i.e. at m/z = 56). In a previous work regarding oxygen-based PPF [16], it was postulated that the $(M\text{-}H)^+$ fragment also produced in allyl alcohol plasma (presenting the same hydrocarbon backbone than allylamine) significantly contributes to the film growth given the high sticking coefficient of unsaturated-based species [49]. In our case, the same mechanism could be proposed considering the close N/C ratios found in the PPF (i.e. ~ 0.27) and in the radical (i.e. 0.33). On the other hand, stable molecules containing the heteroelement are also formed (e.g. $NH_3$ at m/z = 17). Considering that these molecules do not participate to the growth of the layer, their production contributes to decrease the overall nitrogen content in the PPF [16].

**TABLE 1** | Mean score plot (PC1) as a function of $T_S$ resulting from the PCA analysis of the ToF-SIMS data of $NH_2$-PPF (Figure 5).

| | Substrate temperature (°C) | | | | |
|---|---|---|---|---|---|
| | **−10°C** | **0°C** | **10°C** | **23°C** | **45°C** |
| $NH_2$-PPF | 16.7 ± 1.4 | 4.83 ± 0.48 | 2.00 ± 0.92 | −6.32 ± 0.47 | −12.66 ± 0.85 |

**TABLE 2** | Average fragments and their corresponding C/H ratio of the most influential loadings (statistical weight >90%) resulting of the PCA of the ToF-SIMS spectra. The substrate temperature associated with the positive and negative scores is also provided.

| $NH_2$-PPF | Negative loadings | Positive loadings |
|---|---|---|
| Average fragment | $C_{4.09}H_{4.19}$ | $C_{7.50}H_{12.02}$ |
| C/H ratio | 0.978 | 0.624 |
| Substrate temperature | 23°C; 45°C | −10°C; 0°C; 10°C |

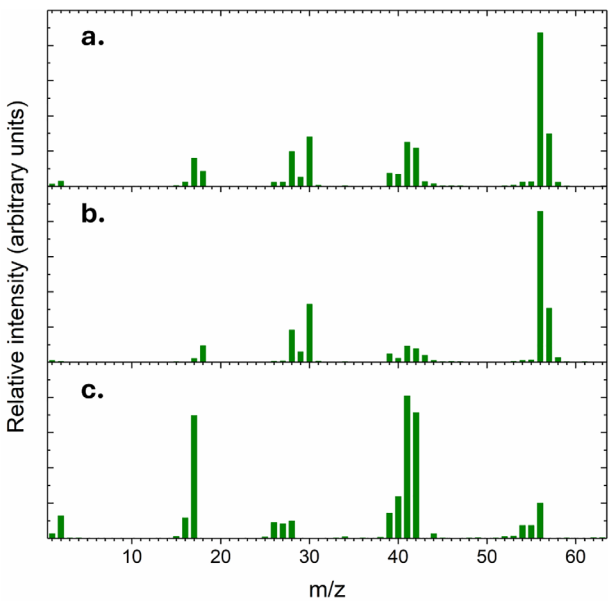


**FIGURE 6** | Mass spectra of allylamine discharge (Plasma ON) (a), allylamine vapor (Plasma OFF) (b) and allylamine plasma treated according to Equation 2 (c).

## 2.1 | Discussion

In order to better understand the collected data, the evolution of the growth rate (R) with $T_S$ was measured. Indeed, previous studies have highlighted that investigating the deposition kinetics vs. the experimental conditions could provide meaningful insights about the growth mechanisms of PPF [17, 50, 51].

As observed in Figure 7a, the growth rate decreases with $T_S$ (i.e. from 5.39 ± 0.33 to 1.568 ± 0.015 nm/min) according to an exponential law (red curve on Figure 7a) as previously observed in the literature for other precursors [15–17, 52].

To understand this behavior, some fundamental concepts of the PPF growth mechanism at the molecular scale have to be discussed. Upon ignition of the plasma, reactive species (mainly radicals and to a lesser extent ions) are generated by electronic collision. Simultaneously, the growing film is continuously bombarded by positive ions (accelerated toward the surface with a kinetic energy typically ranging from 10 to 30 eV) inducing bond breaking at the interface and thus the formation of surface radicals. [48, 53]. The film-forming species from the plasma adsorb and react with the surface-activated sites to form a covalent bond, as described in the Activated Growth Model ("AGM") developed by d'Agostino in the 1980s [9, 54]. From a molecular point of view, the reactive moieties are firstly physisorbed in a weakly-adsorbed state, diffuse along the interface before being chemisorbed through a reaction with a dangling bond [16, 17, 51]. In this context, the residence time ($\tau$), i.e. the average time that the particles spend on the surface before desorption, is a key parameter for the chemical incorporation of the film-forming species. Indeed, increasing (decreasing) $\tau$ results in a higher (lower) probability for the reactive specie to find a chemisorption site before being desorbed.

Based on this approach, R is proportional to the flux of film-forming species toward the interface ($F_R$), the density of surface-activated sites ($S_R$) and the residence time ($\tau$) [16]:

$$R \sim F_R.S_R.\tau = F_R.S_R.\tau_o e^{\frac{-E_{phys}}{k_B T_S}} \quad (3)$$

where $\tau_0$, $E_{phys}$ and $k_B$ correspond to the smallest possible residence time (i.e. the inverse of the vibrational frequency of the surface bond, ~ $10^{-12}$–$10^{-13}$ s), the physisorption energy and the Boltzmann constant, respectively.

Considering Equation 3, it should be mentioned that $F_R$ and $S_R$ directly depend on the fragmentation degree of the precursor in the discharge ($\alpha$) and on the ionic bombardment, respectively.

**TABLE 3** | Attribution of the various peaks observed by mass spectrometry measurement of allylamine-based plasma.

| Allylamine plasma peak attributions | |
|---|---|
| **m/z** | **ions** |
| 2 | $H_2^+$ |
| 14–17 | $NH_{0\text{-}3}^+$ |
| 15–16 | $CH_{3\text{-}4}^+$ |
| 26–30 | $C_2H_{2\text{-}6}^+$; $CNH_{0\text{-}4}^+$ |
| 39–44 | $C_3H_{3\text{-}8}^+$ ; $C_2NH_{1\text{-}6}^+$ |
| 54–56 | $(M\text{-}H)^+$ ; $(M\text{-}2H)^+$ ; $(M\text{-}3H)^+$ |

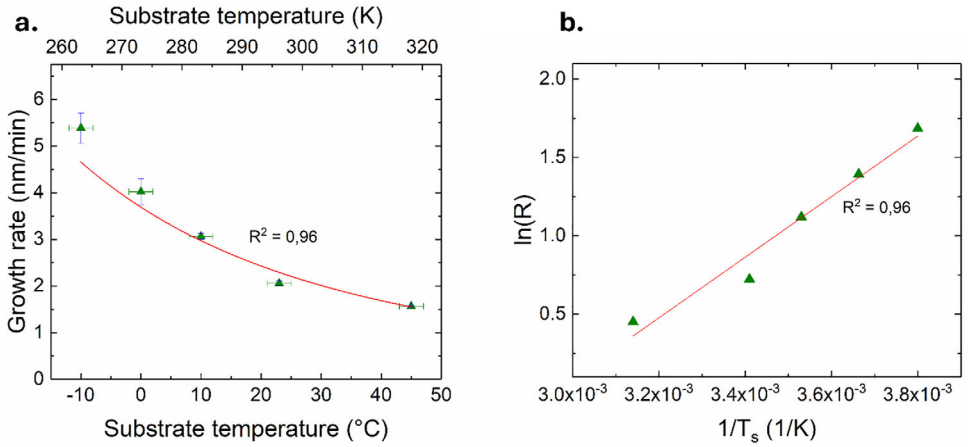


**FIGURE 7** | (a) Growth rate of $NH_2$-PPF as a function of the substrate temperature. The red line is the exponential law fitting. (b) Evolution of ln (R) as a function of inverse $T_S$. The red line is the linear law fitting.

These two parameters are expected to be independent of the substrate thermal conditions. Consequently, only the exponential term depends upon $T_S$, correlating the trend regarding R vs. $T_S$ observed in Figure 7a. Similar equations have successfully described the evolution of R with $T_S$ for PPF of propanethiol, propylamine, methyl methacrylate, allyl alcohol and propanol [16, 17, 52].

Interestingly, $E_{phys}$ can be obtained by plotting ln(R) as a function of $1/T_S$ (see Figure 7b) yielding a value of -0.17 ± 0.02 eV corresponding to typical physisorption energy values [55–57]. $E_{phys}$ can be considered as an apparent physisorption energy of the film-forming species [16].

At this stage, it has been observed that the evolution of $T_T$ and hence, the mechanical properties of the coating, arises from an increase of $\chi$ with $T_S$. On the other side, R varies as a function of $T_S$ and strongly depends on the precursor. In order to understand this observation, the concept of energy density ($\varepsilon$) must be introduced, defined as the energy brought to the growing film through ionic bombardment and normalized with respect to the total amount of matter deposited according to [58, 59]:

$$\varepsilon = \frac{\Gamma_i E_{mean}}{R} \quad (4)$$

where $\Gamma_i$ corresponds to the flux of ions reaching the growing film and $E_{mean}$ the mean energy of the bombarding ions. For several PPF families, a linear correlation has been evidenced between $\chi$ (directly influencing $T_T$ and the mechanical properties) and $\varepsilon$ [59].

Considering our experimental window, only $T_S$ is varied. It can be reasonably assumed that the values of $\Gamma_i$ and $E_{mean}$ (as aforesaid, mainly influenced by the plasma parameters, i.e. electron density and electron temperature) remain stable whatever the thermal conditions of the substrate. On the other hand, as previously shown, R is highly sensitive with regard to $T_S$. According to the Equation 4, $\varepsilon$ is expected to increase with $T_S$ (as R decreases). This

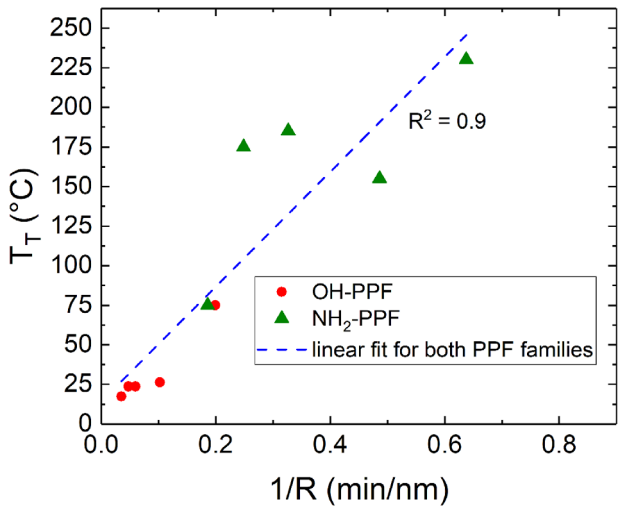


**FIGURE 8** | Evolution of $T_T$ as a function of the inverse of R for allyl alcohol-based PPF (red) and allylamine-based PPF (green). The blue line is the linear fit considering both precursors.

correlates with the increase in $\chi$ with $T_S$, affecting the mobility of the molecular segments and consequently the $T_T$ of the material.

To rationalize these data, the evolution of $T_T$ is plotted as a function of 1/R (i.e. proportional to ε in our experimental window) in Figure 8, along with $T_T$ previously reported for allyl alcohol-PPF synthesized in the same reactor under similar experimental conditions [16]. Interestingly, the evolution of $T_T$ for both precursors follows a similar linear trend as a function of 1/R (blue dashed line, $R^2 = 0.9$), indicating some similarities in their respective growth mechanism. The main difference lies in the 1/R values as for allyl alcohol, the growth kinetic, for similar $T_S$, increases compared to allylamine due to higher physisorption energies (i.e. -0.23 ± 0.01 eV for allyl alcohol and -0.17 ± 0.02 eV for allylamine) and $\alpha$ (i.e. 0.76 ± 0.05% for allyl alcohol vs 0.25 ± 0.05% for allylamine). This set of data clearly reveals that besides the modulation of $T_S$, tuning the chemical function hosted by the precursor allows to enlarge the control over $T_T$ and hence the mechanical properties of the layers.

## 3 | Conclusion

This work explores the influence of the substrate temperature on the chemical composition and mechanical properties of allylamine-based plasma polymers. The objective of this work was to improve our understanding of the relationship between the thermal conditions of the substrate and the growth mechanism.

Although minor mechanical behavior changes (i.e. less than 1 GPa) cannot be excluded, it was shown that the mechanical properties of the PPF are not significantly affected by the substrate temperature, consistently exhibiting an elastic solid behavior with a rigidity modulus of approximately 3 GPa. This trend is correlated with the evolution of the surface transition temperature $T_T$, related to the glass transition of the polymeric film, and systematically above the room temperature. Furthermore, $T_T$ was found to increase with $T_S$ and governed by the cross-linking degree of the coating. The latter directly depends on the energy density brought to the growing film by bombarding ions, which is inversely correlated with deposition kinetics. Interestingly, comparing with already published data, the relationship deduced for allylamine linking the glass transition temperature and the energy density also holds for allyl alcohol suggesting similarities between their respective growth mechanisms. However, these data also highlight major differences in the deposition kinetics under identical experimental conditions, which greatly affect the energy density and, consequently, the mechanical behavior of the polymer film. Therefore, in addition to the substrate temperature, the glass transition can be finely tuned over a wide range (i.e. from 17.5°C to 230°C) and on demand through a judicious choice of the chemical nature of the precursor. The resulting control over the layer viscoelastic properties is of prime interest for numerous applications, notably the conception of flexible electronic components.

The whole set of our data unambiguously provides new insights about the role played by the thermal conditions of the substrate on the mechanistic formation of functionalized plasma polymers offering an additional degree of freedom for material optimization. The analysis of the deposition kinetics as a function of the substrate temperature for a given precursor can serve as a quantitative probe of the interactions between plasma-generated species and the substrate interface. This methodology complements existing macroscopic approaches focused on activation kinetics within the plasma and contributes to a more comprehensive fundamental understanding of the molecular growth mechanism of plasma polymers.

## 4 | Experimental Section/Methods

### 4.1 | Reagents

2-propen-1-amine (99%, Sigma–Aldrich), which will be referenced as allylamine in this work, was used as received on $1 \times 1 cm^2$ silicon pieces cut from wafers. Prior to their introduction in the plasma chamber, the substrates were cleaned with 1-isopropanol three times and dried under a nitrogen flow.

### 4.2 | Plasma Polymerization Method

Plasma polymer film growth was carried out in a metallic deposition chamber (65 cm in length and 35 cm in diameter) with a residual pressure of less than $2.10^{-6}$ Torr. The vacuum was ensured by a combination of turbomolecular and primary pumps. A more detailed description of the plasma chamber can be found elsewhere. (1) The reactor consists in an internal one-turn inductive copper coil (10 cm in diameter) cooled with water connected to an Advanced Energy Radiofrequency (13.56 MHz) power supply with a matching network. For all the experiments, the dissipated power and the precursor flow rate were 40 W and 10 sccm, respectively. The distance separating the substrate from the coil was fixed at 10 cm. The working pressure was 40 mTorr and was controlled during the process with a throttle valve connected to a capacitive gauge. The substrate temperature was controlled by a combination of liquid nitrogen flow in the manipulator (for cooling) and electrical resistances in the substrate holder (heating) coupled with a thermocouple, also inside the substrate holder. This system allowed to control the temperature with a precision of ±1°C. Five temperatures have been investigated in this work, namely -10°C, 0°C, 10°C, 23°C, and 45°C. Before each deposition, the substrate temperature was stabilized for 30 min to ensure the thermal equilibrium between the silicon substrate and the heating/cooling system. For the sake of simplicity, PPF synthesized with allylamine at a substrate temperature "X"°C will be noted $NH_2$-$PPF_{X°C}$ in this work.

### 4.3 | Thickness Measurements

The deposited film thicknesses have been acquired by scratching the coating surface with a scalpel blade and measuring the depth of the produced step by AFM measurement five times. The apparatus consists of a Bruker Multimode 8 microscope (Tapping Mode) associated with a Nanoscope III controller. The growth rate was obtained from the measured thickness vs the deposition time. Growth rate error margins are determined from the error in PPF thicknesses, calculated from a series of five measurements.

### 4.4 | XPS Measurements

The chemical composition of the PPF has been investigated by means of XPS (X-ray Photoelectron Spectroscopy). The measurements were carried out by a PHI 5000 VersaProbe apparatus under a pressure of $5.10^{-9}$ Torr. The photon source was a monochromatized Al K$\alpha$ line (1486.6 eV). The emitted photoelectrons were collected with an angle of 45° with respect to the surface. XPS spectra were acquired with a resolution of 0.2 eV. Charge minimization was ensured using a dual-charge compensation system with a combination of low energy electrons and argon ions. Analysis was performed directly after the PPF synthesis to ensure minimal air contamination. Each sample was analyzed at three different areas to ensure its homogeneity. XPS spectra were calibrated by setting the C1s peak to a binding energy of 285.0 eV. High resolution C1s and N1s spectra were curve fitted using Multi-Pak software and considering a Gaussian-Lorentzian function (70% Gaussian) with a full width at half-maximum of 1.0–1.5 eV.

### 4.5 | Cross-Linking Degree Evaluation

The cross-linking degrees were studied with the use of ToF-SIMS measurement. Samples were probed immediately after their synthesis to avoid air contamination. Static ToF-SIMS data were acquired in positive mode at room temperature with a ToF-SIMS IV instrument supplied by ION TOF GmbH using a pulsed 10 keV $Ar^+$ ion beam (0.75 pA) rastering a scan area of 300×300 $\mu m^2$ eight time for each sample. The ToF-SIMS mass spectra were normalized to the total ion count number and analyzed with the help of a statistical method called Principal Component Analysis (PCA) using the SIMCA-13 software supplied by Umetrics (Sweden).

PCA is a multivariate analysis technique aiming at summarizing the variance patterns within a dataset. The variance in the data describes the differences between the samples. For ToF-SIMS data, these differences come from changes in the relative intensity of the peaks between the sample spectra. Using PCA, a new set of axes called principal components (PCi) is created, defining the directions of the major variations within the data set. PC1 describes the line that best approximates the data. Usually, one PCi is not enough to model the variance of a data set. A second PCi (PC2), orthogonal to PC1, is then calculated to improve the data approximation and so on. The results are then interpreted using specific concepts namely the "scores" and the "loadings". The scores describe the relationship between the samples synthesized at each $T_S$, while the loadings reveal the ionized fragments responsible for the differences between the samples. More information about this multivariate analysis method and its uses in plasma investigation can be found elsewhere [27, 40, 41].

### 4.6 | Surface Transition Temperature Evaluation

Glass transition temperatures of the samples have been estimated with a recently developed method based on ToF-SIMS measurements [30, 60]. Static ToF-SIMS data have been acquired with a ToF-SIMS V instrument supplied by ION TOF GmbH. An Ar gas cluster ion beam (Ar-GCIB) with a cluster distribution centered on $Ar_{3000}{}^+$ was raster-scanned over an area of 500 × 500 $\mu m^2$ (128 × 128 data points). Ar cluster ions were accelerated toward the surface with an energy of 10 keV. A low-energy (5 eV) electron flood gun was used to avoid charging effects of the probed sample. Before each analysis, the analyte temperature was stabilized 20 min prior to analysis to ensure the thermal equilibrium of the PPF and potential surface contamination were removed by pre-sputtering of $2 \times 10^{13}$ $Ar_{3000}{}^+/cm^2$ in DC mode over an area of 1000×1000 $\mu m^2$. The thickness of the probed PPF was fixed at 220 nm to avoid any substrate effect on the measurement. Analysis of the ToF-SIMS data, specifically the $Ar_2{}^+$ and $Ar_3{}^+$ peak intensities, was exploited to determine the surface transition temperature ($T_T$), strongly correlated to the bulk glass transition temperature ($T_g$).

### 4.7 | Mechanical and Viscoelastic Characterization

The PPF mechanical properties were probed by Peak-Force Tapping Quantitative Nanomechanical Mapping (PF-QNM). [61, 62]. Measurements were performed using a Bruker AFM ICON Dimension equipped with a Nanoscope 6 Controller. PF-QNM data were collected using pre-calibrated AFM tips (RTESPA300-30) supplied by Bruker with a calibrated spring constant k of ± 50 N/m and tip radius of ± 25 nm. The rigidity modulus values were extracted by fitting part of the retract curve with the Johnson-Kendall-Roberts (JKR) model. JKR previously proved to be effective in the analysis of deformable materials, notably PPF [18]. More information about the JKR theory and its describing equations can be found elsewhere [26]. Three measurements have been made for each sample using different areas. The thickness of the probed PPF was fixed at 220 nm to avoid any impact of the substrate on the AFM measurements.

### 4.8 | FTIR Characterization

Infrared measurements were performed in Attenuated Total Reflectance mode (ATR) using a ALPHA II Compact FT-IR Spectrometer supplied by Bruker. For each sample, three spectra were acquired to ensure the sample homogeneity and then averaged. Spectral background removal was performed using the Sensitive Nonlinear Iterative Peak-clipping (SNIP) algorithm with 8 iterations [63].

### 4.9 | Mass Spectrometry

The plasma composition was probed with a quadrupole HAL EQP 1000 mass spectrometer provided by Hidden Analytical. A 100 μm extraction orifice connected the spectrometer to the plasma chamber. The neutral plasma species were investigated in residual gas analysis mode (RGA). Radicals and molecules were ionized by electron impact (EI) with a low kinetic energy of 20 eV to limit their fragmentation in the spectrometer. For the sake of clarity, the mass spectra are presented from m/z = 1 to 65 as no significant peaks are observed for a higher value of m/z.

#### Acknowledgements

This publication is supported by the French Community of Belgium ("Communauté française de Belgique") through a FRIA grant. The research at LPNE is partly supported by F.R.S.– FNRS PDR Project, Belgium (40007942) and F.R.S.– FNRS Grands Equipements Project (40007941) (Belgium).

#### Funding

This publication is supported by the French Community of Belgium ("Communauté française de Belgique") through a FRIA grant. The research at LPNE is partly supported by F.R.S.– FNRS PDR Project, Belgium (40007942) and F.R.S.– FNRS Grands Equipements Project (40007941) (Belgium).

#### Conflicts of Interest

The authors declare no conflicts of interest.

#### Data Availability Statement

The data that support the findings of this study are available from the corresponding author upon reasonable request.

## References


1. D. Thiry, N. Britun, S. Konstantinidis, et al., "Experimental and Theoretical Study of the Effect of the Inductive-to-Capacitive Transition in Propanethiol Plasma Polymer Chemistry," *The Journal of Physical Chemistry C* 117 (2013): 9843–9851, https://doi.org/10.1021/jp400829z.

2. L. Denis, P. Marsal, Y. Olivier, et al., "Deposition of Functional Organic Thin Films by Pulsed Plasma Polymerization: A Joint Theoretical and Experimental Study," *Plasma Processes and Polymers* 7 (2010): 172–181, https://doi.org/10.1002/ppap.200900131.

3. A. Fahmy, R. Mix, A. Schönhals, and J. F. Friedrich, "Structure–Property Relationship of Thin Plasma Deposited Poly(allyl alcohol) Films," *Plasma Chemistry and Plasma Processing* 31 (2011): 477–498, https://doi.org/10.1007/s11090-011-9297-0.

4. S. A. Voronin, M. Zelzer, C. Fotea, M. R. Alexander, and J. W. Bradley, "Pulsed and Continuous Wave Acrylic Acid Radio Frequency Plasma Deposits: Plasma and Surface Chemistry," *The Journal of Physical Chemistry B* 111 (2007): 3419–3429, https://doi.org/10.1021/jp068488z.

5. E. Makhneva, A. Manakhov, P. Skládal, and L. Zajíčková, "Development of Effective QCM Biosensors by Cyclopropylamine Plasma Polymerization and Antibody Immobilization Using Cross-linking Reactions," *Surface and Coatings Technology* 290 (2016): 116–123, https://doi.org/10.1016/j.surfcoat.2015.09.035.

6. P. Sťahel, V. Mazánková, K. Tomečková, et al., "Atmospheric Pressure Plasma Polymerized Oxazoline-Based Thin Films—Antibacterial Properties and Cytocompatibility Performance," *Polymers* 11 (2019): 2069, https://doi.org/10.3390/polym11122069.

7. B. Joseph, N. Ninan, R. M. Visalakshan, et al., "Insights Into the Biomechanical Properties of Plasma Treated 3D Printed PCL Scaffolds Decorated With Gold Nanoparticles," *Composites Science and Technology* 202 (2021): 108544, https://doi.org/10.1016/j.compscitech.2020.108544.

8. N. Inagaki, *Plasma Surface Modification and Plasma Polymerization* (CRC Press Inc, 1996), https://doi.org/10.1201/9781498710831.

9. H. Biederman, *Plasma Polymer Films* (Imperial College Press, 2004), https://doi.org/10.1142/p336.

10. L. M. Han, R. B. Timmons, and W. W. Lee, "Pulsed Plasma Polymerization of an Aromatic Perfluorocarbon Monomer: Formation of Low Dielectric Constant, High Thermal Stability Films," *Journal of Vacuum Science & Technology B: Microelectronics and Nanometer Structures Processing, Measurement, and Phenomena* 18 (2000): 799–804, https://doi.org/10.1116/1.591279.

11. F. Fally, C. Doneux, J. Riga, and J. J. Verbist, "Quantification of the Functional Groups Present at the Surface of Plasma Polymers Deposited From Propylamine, Allylamine, and Propargylamine," *Journal of Applied Polymer Science* 56 (1995): 597–614, https://doi.org/10.1002/app.1995.070560509.

12. J. Ryssy, E. Prioste-Amaral, D. F. N. Assuncao, et al., "Chemical and Physical Processes in the Retention of Functional Groups in Plasma Polymers Studied by Plasma Phase Mass Spectroscopy," *Physical Chemistry Chemical Physics* 18 (2016): 4496–4504, https://doi.org/10.1039/C5CP05850C.

13. D. Thiry, M. Pouyanne, D. Cossement, A. Hemberg, and R. Snyders, "Surface Engineering of Bromine-Based Plasma Polymer Films: A Step Toward High Thiol Density Containing Organic Coatings," *Langmuir* 34 (2018): 7655–7662, https://doi.org/10.1021/acs.langmuir.8b01045.

14. J. Petersen, J. Bardon, A. Dinia, D. Ruch, and N. Gherardi, "Organosilicon Coatings Deposited in Atmospheric Pressure Townsend Discharge for Gas Barrier Purpose: Effect of Substrate Temperature on Structure and Properties," *ACS Applied Materials & Interfaces* 4 (2012): 5872–5882, https://doi.org/10.1021/am3015229.

15. H. Yasuda and C. R. Wang, "Plasma Polymerization Investigated by the Substrate Temperature Dependence," *Journal of Polymer Science Part A-1, Polymer Chemistry* 23 (1985): 87–106, https://doi.org/10.1002/pol.1985.170230110.

16. R. Dantinne, N. Vinx, P. Leclère, et al., "Investigating the Influence of the Substrate Temperature and the Organic Precursor on the Mechanical Properties of Low-Pressure Plasma Polymer Films," *Plasma Processes and Polymers* 21 (2024): 2400166, https://doi.org/10.1002/ppap.202400166.

17. N. Vinx, P. Leclère, C. Poleunis, et al., "The Influence of the Substrate Temperature on the Growth Mechanism of Amine- and Thiol-based Plasma Polymers: A Comparative study," *Plasma Processes and Polymers* 21 (2023): 2300138, https://doi.org/10.1002/ppap.202300138.

18. N. Vinx, P. Damman, P. Leclère, et al., "Investigating the Relationship Between the Mechanical Properties of Plasma Polymer-Like Thin Films and Their Glass Transition Temperature," *Soft Matter* 17 (2021): 10032–10041, https://doi.org/10.1039/D1SM01134K.

19. N. Vinx, D. Tromont, A. Chauvin, P. Leclère, R. Snyders, and D. Thiry, "Designing Nanostructured Organic-Based Material by Combining Plasma Polymerization and the Wrinkling Approach," *Langmuir* 39 (2023): 15231–15237, https://doi.org/10.1021/acs.langmuir.3c01873.

20. S. A. Raut, N. Vinx, D. Tromont, et al., "Unlocking the Potential of Liquid Plasma Polymer Films: Characterizing Aging Effects and Their Impact on the Wrinkling Phenomenon," *Langmuir* 40 (2024): 14633–14640, https://doi.org/10.1021/acs.langmuir.4c01552.

21. D. Thiry, N. Vinx, P. Damman, et al., "The Wrinkling Concept Applied to Plasma-Deposited Polymer-Like Thin Films: A Promising Method for the Fabrication of Flexible Electrodes," *Plasma Processes and Polymers* 17 (2020): 2000119, https://doi.org/10.1002/ppap.202000119.

22. B. Finke, H. Rebl, F. Hempel, et al., "Aging of Plasma-Polymerized Allylamine Nanofilms and the Maintenance of Their Cell Adhesion Capacity," *Langmuir* 30 (2014): 13914–13924, https://doi.org/10.1021/la5019778.

23. X. Liu, Q. Feng, A. Bachhuka, and K. Vasilev, "Surface Modification by Allylamine Plasma Polymerization Promotes Osteogenic Differentiation of Human Adipose-Derived Stem Cells," *ACS Applied Materials & Interfaces* 6 (2014): 9733–9741, https://doi.org/10.1021/am502170s.

24. S. Swaraj, U. Oran, A. Lippitz, J. F. Friedrich, and W. E. S. Unger, "Study of Influence of External Plasma Parameters on Plasma Polymerised Films Prepared From Organic Molecules (acrylic acid, allyl alcohol, allyl amine) Using XPS and NEXAFS," *Surface and Coatings Technology* 200 (2005): 494–497, https://doi.org/10.1016/j.surfcoat.2005.01.083.

25. A. Kwaśniewska, M. Świetlicki, A. Prószyński, and G. Gładyszewski, "The Quantitative Nanomechanical Mapping of Starch/Kaolin Film Surfaces by Peak Force AFM," *Polymers* 13 (2021): 244, https://doi.org/10.3390/polym13020244.

26. K. L. Johnson, K. Kendall, and A. D. Roberts, "Surface Energy and the Contact of Elastic Solids," *Proceedings of the Royal Society of London A Mathematical and Physical Sciences* 324 (1971): 301–313, https://doi.org/10.1098/rspa.1971.0141.

27. S. Ligot, E. Bousser, D. Cossement, et al., "Correlation between Mechanical Properties and Cross-Linking Degree of Ethyl Lactate Plasma Polymer Films," *Plasma Processes and Polymers* 12 (2015): 508–518, https://doi.org/10.1002/ppap.201400162.

28. J. Bicerano, "Glass Transition," in *Encyclopedia of Polymer Science and Technology* (John Wiley & Sons, Inc., 2001), 655–677, https://doi.org/10.1002/0471440264.pst149.

29. V. R. Gowariker, J. Sreedar, and N. V. Viswanathan, *Polymer Science* (Halsted Press, 1986).

30. C. Poleunis, V. Cristaudo, and A. Delcorte, "Temperature Dependence of $Ar_n^+$ Cluster Backscattering From Polymer Surfaces: A New Method to Determine the Surface Glass Transition Temperature," *Journal of the American Society for Mass Spectrometry* 29 (2018): 4–7, https://doi.org/10.1007/s13361-017-1840-7.

31. K. L. Ngai, "The Glass Transition and the Glassy State," in *Physical Properties of Polymers* (Cambridge University Press, 2004): 72–152, https://doi.org/10.1017/CBO9781139165167.003.

32. T. R. Gengenbach and H. J. Griesser, "Deposition Conditions Influence the Postdeposition Oxidation of Methyl Methacrylate Plasma Polymer Films," *Journal of Polymer Science Part A: Polymer Chemistry* 36 (1998): 985–1000, https://doi.org/10.1002/(SICI)1099-0518(19980430)36:6⟨985::AID-POLA14⟩3.0.CO;2-H.

33. A. J. Beck, S. Candan, R. D. Short, A. Goodyear, and N. S. J. Braithwaite, "The Role of Ions in the Plasma Polymerization of Allylamine," *The Journal of Physical Chemistry B* 105 (2001): 5730–5736, https://doi.org/10.1021/jp0043468.

34. L. Denis, D. Cossement, T. Godfroid, et al., "Synthesis of Allylamine Plasma Polymer Films: Correlation Between Plasma Diagnostic and Film Characteristics," *Plasma Processes and Polymers* 6 (2009): 199–208, https://doi.org/10.1002/ppap.200800137.

35. A. Choukourov, H. Biederman, D. Slavinska, et al., "Mechanistic Studies of Plasma Polymerization of Allylamine," *The Journal of Physical Chemistry B* 109 (2005): 23086–23095, https://doi.org/10.1021/jp0535691.

36. S. Candan, "Radio Frequency-Induced Plasma Polymerization of Allyl Alcohol and 1-propanol," *Turkish Journal of Chemistry* 26 (2002): 783–791.

37. M. B. Larsen, S.-J. Wang, and M. A. Hillmyer, "Poly(allyl alcohol) Homo- and Block Polymers by Postpolymerization Reduction of an Activated Polyacrylamide," *Journal of the American Chemical Society* 140 (2018): 11911–11915, https://doi.org/10.1021/jacs.8b07542.

38. L. Denis, D. Thiry, D. Cossement, et al., "Towards the Understanding of Plasma Polymer Film Behaviour in Ethanol: A Multi-technique Investigation," *Progress in Organic Coatings* 70 (2011): 134–141, https://doi.org/10.1016/j.porgcoat.2010.11.006.

39. A. Choukourov, H. Biederman, I. Kholodkov, D. Slavinska, M. Trchova, and A. Hollander, "Properties of Amine-Containing Coatings Prepared by Plasma Polymerization," *Journal of Applied Polymer Science* 92 (2004): 979–990, https://doi.org/10.1002/app.13387.

40. L. Eriksson, E. Johansson, N. Kettaneth-Wold, et al., *Multi- and Megavariate Data Analysis Basic Principles and Applications*, Vol. 1 (Umetrics Academy (Umetrics AB), 2006).

41. D. Cossement, F. Renaux, D. Thiry, S. Ligot, R. Francq, and R. Snyders, "Chemical and Microstructural Characterizations of Plasma Polymer Films by Time-of-Flight Secondary Ion Mass Spectrometry and Principal Component Analysis," *Applied Surface Science* 355 (2015): 842–848, https://doi.org/10.1016/j.apsusc.2015.07.066.

42. D. Thiry, R. Francq, D. Cossement, M. Guillaume, J. Cornil, and R. Snyders, "A Detailed Description of the Chemistry of Thiol Supporting Plasma Polymer Films," *Plasma Processes and Polymers* 11 (2014): 606–615, https://doi.org/10.1002/ppap.201400015.

43. V. Cristaudo, D. Merche, C. Poleunis, et al., "Ex-Situ SIMS Characterization of Plasma-Deposited Polystyrene Near Atmospheric Pressure," *Applied Surface Science* 481 (2019): 1490–1502, https://doi.org/10.1016/j.apsusc.2019.03.032.

44. F. J. Aparicio, D. Thiry, P. Laha, and R. Snyders, "Wide Range Control of the Chemical Composition and Optical Properties of Propanethiol Plasma Polymer Films by Regulating the Deposition Temperature," *Plasma Processes and Polymers* 13 (2016): 814–822, https://doi.org/10.1002/ppap.201500212.

45. H. Kobayashi, A. T. Bell, and M. Shen, "Plasma Polymerization of Saturated and Unsaturated Hydrocarbons," *Macromolecules* 7 (1974): 277–283, https://doi.org/10.1021/ma60039a005.

46. R. Snyders, D. Hegemann, D. Thiry, O. Zabeida, J. Klemberg-Sapieha, and L. Martinu, "Foundations of Plasma Enhanced Chemical Vapor Deposition of Functional Coatings," *Plasma Sources Science and Technology* 32 (2023): 074001, https://doi.org/10.1088/1361-6595/acdabc.

47. J. Friedrich, "Mechanisms of Plasma Polymerization—Reviewed From a Chemical Point of View," *Plasma Processes and Polymers* 8 (2011): 783–802, https://doi.org/10.1002/ppap.201100038.

48. D. Thiry, S. Konstantinidis, J. Cornil, and R. Snyders, "Plasma Diagnostics for the Low-Pressure Plasma Polymerization Process: A Critical Review," *Thin Solid Films* 606 (2016): 19–44, https://doi.org/10.1016/j.tsf.2016.02.058.

49. C. Hopf, T. Schwarz-Selinger, W. Jacob, and A. Keudell, "Surface Loss Probabilities of Hydrocarbon Radicals on Amorphous Hydrogenated Carbon Film Surfaces," *Journal of Applied Physics* 87 (2000): 2719–2725, https://doi.org/10.1063/1.372246.

50. D. Hegemann, "Macroscopic Investigation of Reaction Rates Yielding Plasma Polymer Deposition," *Journal of Physics D: Applied Physics* 46 (2013): 205204, https://doi.org/10.1088/0022-3727/46/20/205204.

51. A. Keudell, "Surface Processes During Thin-Film Growth," *Plasma Sources Science and Technology* 9 (2000): 455–467, https://doi.org/10.1088/0963-0252/9/4/302.

52. T. B. Casserly and K. K. Gleason, "Effect of Substrate Temperature on the Plasma Polymerization of Poly(methyl methacrylate)," *Chemical Vapor Deposition* 12 (2006): 59–66, https://doi.org/10.1002/cvde.200506409.

53. D. Thiry, F. Reniers, and R. Snyders, "A Joint Mechanistic Description of Plasma Polymers Synthesized at Low and Atmospheric Pressure," in *Surface Modification of Polymers* (Wiley-VCH Verlag GmbH & Co. KGaA, 2019), 67–106, https://doi.org/10.1002/9783527819249.ch3.

54. R. D'Agostino, F. Cramarossa, F. Fracassi, et al., "Polymer Film Formation in $C_2F_6$ $H_2$ Discharges," *Thin Solid Films* 143 (1986): 163–175, https://doi.org/10.1016/0040-6090(86)90384-6.

55. B. A. De Moor, M.-F. Reyniers, and G. B. Marin, "Physisorption and Chemisorption of Alkanes and Alkenes in H-FAU: A Combined Ab Initio–Statistical Thermodynamics Study," *Physical Chemistry Chemical Physics* 11 (2009): 2939, https://doi.org/10.1039/b819435c.

56. A. S. Raman and A. Vojvodic, "Energy Trends in Adsorption at Surfaces," in *Handbook of Materials Modeling* (Springer International Publishing, 2020), 1321–1341, https://doi.org/10.1007/978-3-319-44680-6_2.

57. K. Horn and M. Scheffler, *Electronic Structure* (Elsevier Science, 2000).

58. D. Hegemann, U. Schütz, and E. Körner, "Macroscopic Approach to Plasma Polymerization Using the Concept of Energy Density," *Plasma Processes and Polymers* 8 (2011): 689–694, https://doi.org/10.1002/ppap.201000211.

59. D. Hegemann, E. Körner, N. Blanchard, M. Drabik, and S. Guimond, "Densification of Functional Plasma Polymers by Momentum Transfer During Film Growth," *Applied Physics Letters* 101 (2012): 211603, https://doi.org/10.1063/1.4767999.

60. M. Chundak, C. Poleunis, V. Delmez, et al., "Argon Gas Cluster Fragmentation and Scattering as a Probe of the Surface Physics of Thermoset Polymers," *Applied Surface Science* 533 (2020): 147473, https://doi.org/10.1016/j.apsusc.2020.147473.

61. P. Trtik, J. Kaufmann, and U. Volz, "On the Use of Peak-force Tapping Atomic Force Microscopy for Quantification of the Local Elastic Modulus in Hardened Cement Paste," *Cement and Concrete Research* 42 (2012): 215–221, https://doi.org/10.1016/j.cemconres.2011.08.009.

62. B. Pittenger, S. Osechinskiy, D. Yablon, and T. Mueller, "Nanoscale DMA With the Atomic Force Microscope: A New Method for Measuring Viscoelastic Properties of Nanostructured Polymer Materials," *Jom Journal of the Minerals Metals and Materials Society* 71 (2019): 3390–3398, https://doi.org/10.1007/s11837-019-03698-z.

63. M. Morháč and V. Matoušek, "Peak Clipping Algorithms for Background Estimation in Spectroscopic Data," *Applied Spectroscopy* 62 (2008): 91–106, https://doi.org/10.1366/000370208783412762.

## Supporting Information

Additional supporting information can be found online in the Supporting Information section.

**Supporting File**: admi70484-sup-0001-SuppMat.docx.